A Universal Strategy for Multi-Color Organic Circularly Polarized Afterglow Materials with High Dissymmetry Factor

Chenjia Yin[1], Zi-Ang Yan[1], Honglong Hu[1,2], Ping Jiang[1], Zhuoran Xu[1], He Tian[1], and Xiang Ma[1]*

[1]Key Laboratory for Advanced Materials and Feringa Nobel Prize Scientist Joint Research Center, Frontiers Science Center for Materiobiology and Dynamic Chemistry, Institute of Fine Chemicals, School of Chemistry and Molecular Engineering, East China University of Science and Technology, Meilong Road 130, Shanghai 200237, P. R. China

Chenjia Yin, Zi-Ang Yan, Honglong Hu, Ping Jiang, Zhuoran Xu, He Tian, and Xiang Ma

*E-mail: maxiang@ecust.edu.cn

[2]School of Physics, East China University of Science & Technology, Meilong Road 130, Shanghai 200237, P. R. China

Honglong Hu

Abstract

Materials with pure organic circularly polarized afterglow (CPA) are notable for their multi-dimensional optical characteristics due to their time-dependent afterglow and polarization properties. These attributes endow them with exceptional appeal and value in the realms of information storage and anti-counterfeiting measures. Currently, there are limited studies on multi-color CPA materials with both high dissymmetry factor (g_{lum}) values and long lifetimes. Here, we propose a universal strategy to prepare multi-color CPA materials spanning from blue to red, with an ultralong emission lifetime of over 6 s and a g_{lum} of up to 10^0 (the highest g_{lum} was 1.90). This strategy leverages the mechanism of radiative energy transfer and selective reflection of cholesteric liquid crystals. Through multi-layered assembly, our method offers a simple and universal means of constructing organic CPA materials for multi-dimensional information encryption.

Introduction

Pure organic room temperature phosphorescence (RTP) is burgeoning in fields such as bioimaging[1,2], sensing[3,4], and anti-counterfeiting[5,6] due to their large Stokes shifts, long emission lifetimes, and low toxicity. Organic ultralong RTP (OU-RTP) materials have an afterglow that can be seen with naked eye, expanding the dimensions of optional signals. Unlike linearly polarized light, circularly polarized luminescence (CPL) is characterized by an electric field vector that rotates circularly around the propagation axis, offering enhanced resolution and signal fidelity in optical imaging and communication systems[7,8]. The combination of persistent luminescence properties of OU-RTP and circular polarization can offer stable polarized light signals over an extended period. This integration further expands the dimensions of luminescent signals, enhances the stability and reliability of stored information, and enables the development of highly sensitive and selective optical sensors.

The dissymmetry factor (g_{lum}) is a crucial parameter for quantifying CPL, which is defined as $g_{lum} = 2(I_L - I_R)/(I_L + I_R)$, where I_L and I_R signify the emission intensity of left-handed and right-handed CPL, respectively. This scale measures the chirality of the excited-state chiroptical information, where -2 represents pure right-handed CPL, and +2 signifies pure left-handed CPL. Despite various proposed methods for enhancing g_{lum} values of organic circularly polarized afterglow (CPA) materials — such as crystal engineering[9], copolymerization[10,11], doping[12], and chiral supramolecular assembly[13-15] — achieving materials with both ultralong lifetime and high g_{lum} values remains challenging, let alone tunable emission colors.

Integrating luminescent materials and cholesteric liquid crystals (CLCs) is a promising approach to achieve high g_{lum} values in CPL systems according to prior studies[16,17]. CLCs, characterized by their chiral helical structure, can selectively reflect CPL in accordance with their helical pitch; positioning them as suitable candidates for high-g_{lum} CPL generation. Nonetheless, their fluidity and reliance on rigid substrates, as well as their lack of chemical stability and mechanical strength, seriously hindered the practical viability of this technology in a variety of applications. In contrast, cholesteric liquid crystal polymer (CLCP) films, with their flexibility, offer an alternative that overcomes these limitations[18].

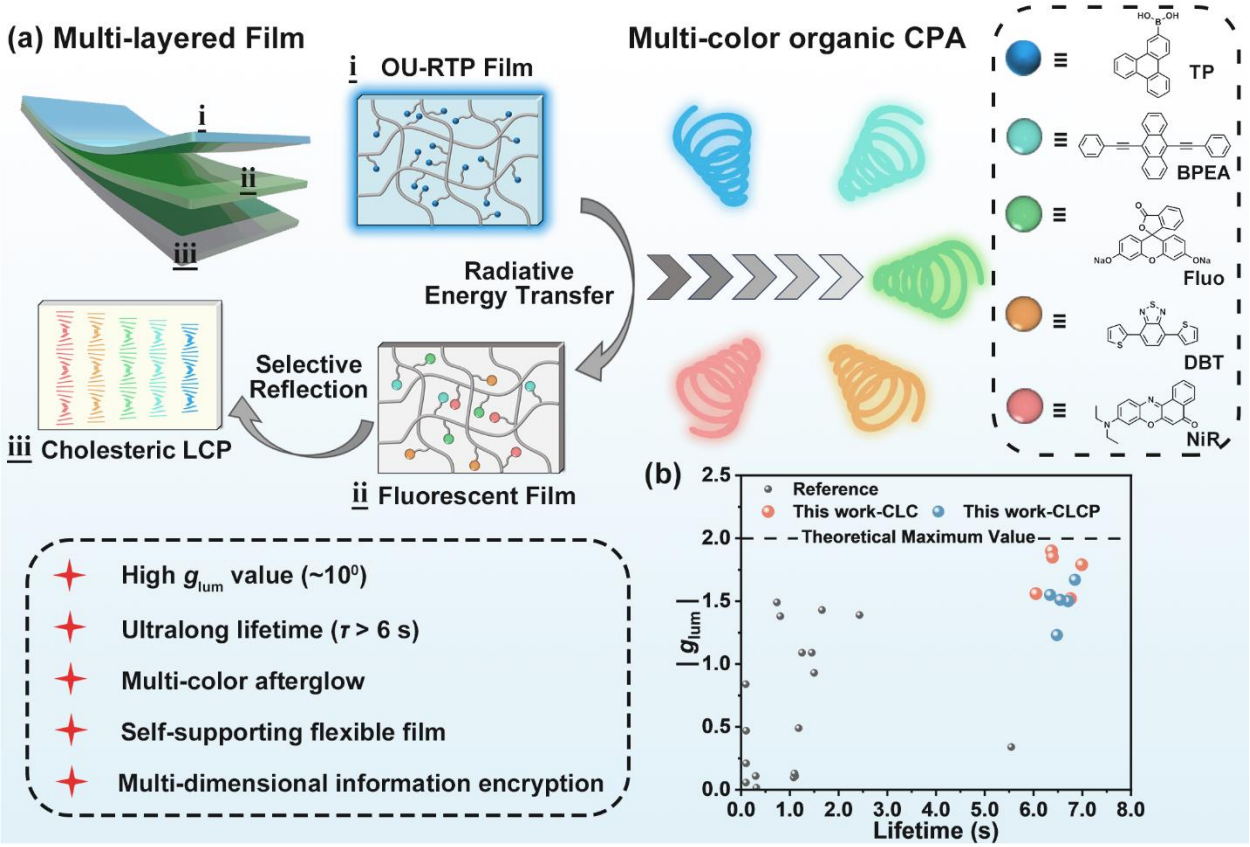

Fig. 1: Strategy and performance of pure organic CPA materials. (a) Schematic illustration of the assembly of multi-layered films and the formation of multi-color pure organic CPA. (b) CPL performance of pure organic CPA materials based on CLCs (grey spheres refer to the organic CPA data from published results[19-22,27-37])

Currently, researchers[19,20] are actively leveraging CLCP to fabricate CPA with high g_{lum} values. For example, Zhao[21] embedded phosphorescent polymers into CLCs, yielding a green CPA with a luminescence lifetime of 0.735 s and a g_{lum} value of 1.49 after UV-induced polymerization. Deng's team[22] achieved a blue CPA with a 2.43 s lifetime and a g_{lum} value of 1.57 by integrating CLCs doped with chiral fluorescent helical polyacetylene with phosphorescent films. However, the red CPA material they attained had a short lifetime of 95 ms with a g_{lum} value of -0.84. It is clear that the development of CPA materials with ultralong lifetimes (τ > 5 s) and high g_{lum} values (~ 10^0) is a substantial challenge, not to mention the realization of full-color tunable pure organic CPA materials. In this work, a universal strategy for constructing pure

organic CPA materials with high g_{lum} values was reported, which was based on radiative energy transfer and the selective reflection mechanism of CLCs/CLCPs. The preparation of an energy donor layer was initiated by incorporating triphenylen-2-ylboronic acid (TP) into polyvinyl alcohol (PVA), resulting in a composite material designated as TP-PVA. Subsequently, four fluorescent dyes were selected, namely 9,10-bis(phenylethynyl)anthracene (BPEA), fluorescein sodium (Fluo), 4,7-di(thiophen-2-yl)benzo[*c*][1,2,5]thiadiazole (DBT), and nile red (NiR), whose absorption spectra overlap with the phosphorescence spectrum of TP-PVA. These materials were incorporated into polymethyl methacrylate (PMMA) or polyvinyl butyral (PVB) matrix, serving as the energy acceptor layers. Besides, CLCs/CLCPs with different photonic band gaps (PBGs) were fabricated by modulating the concentration of chiral dopants within the CLCs/CLCPs. A triple-layered system was sequentially integrated utilizing drop casting and tableting techniques. Notably, unlike Förster resonance energy transfer (FRET), radiative energy transfer retains the ultralong lifetime of 6.37 s of the donor (TP-PVA). After turning off 254 nm excitation, the afterglow from TP-PVA acted as a light source, continually exciting the acceptor layers[23], aligning the lifetime of acceptor with that of donor, and enabling tunable color ultralong afterglow. Furthermore, full-color CPL was attained by the selective reflection mechanism of CLCP films in conjunction with PBGs that match the afterglow emission wavelengths. This resulted in ultra-long lifetimes (over 6 s) and high g_{lum} values (up to 1.90) across 420 – 800 nm, surpassing prior pure organic CPA materials (Fig. 1b and Table S1). This innovation facilitates multi-dimensional information encryption, harnessing the distinctive features of the approach, such as ultralong lifetimes, high g_{lum} values, and multicolor emissions.

Results

Organic Ultralong RTP Polymer Film. TP was chosen as the luminescent donor for radiative energy transfer because it is a polycyclic aromatic hydrocarbon, which endows it with planar rigidity and low spin-orbit coupling. These attributes contribute to a significantly slow radiation transition from T_1 to S_0, thereby facilitating the realization of ultralong lifetime[24]. TP was doped into PVA, a rigid polymer matrix known for its abundant hydroxyl groups. Under alkaline conditions, B-O covalent bonds formed between the boron

atoms and the hydroxyl oxygen of PVA, further restricting molecular thermal motion and inhibiting non-radiative transitions[25]. The yield of the dehydration condensation reaction was proven to be 78% through UV–vis absorption measurements (Fig. S1). The fluorescence spectrum of the TP-PVA film exhibited a blue-purple emission peak at approximately 367 nm with a lifetime of 22.4 ns. (Figs. 2a and S2). The delayed emission spectrum showed that the blue emission at 473 nm belongs to RTP. Remarkably, the phosphorescence lifetime of TP-PVA was as high as 6.37 s, with visible blue afterglow lasting for 36 s under ambient conditions (Fig. 2b). Moreover, TP-PVA also demonstrated satisfactory phosphorescence quantum yield (53.9%). These results collectively demonstrate that TP-PVA serves as an excellent energy transfer donor.

Construction of Energy Transfer Systems. To construct multi-color ultralong afterglow, a series of fluorescent dyes with absorption overlap with the blue phosphorescence of TP-PVA were selected(Fig. 2c), including BPEA, Fluo, DBT, and NiR. Among them, BPEA, DBT, and NiR were incorporated into PMMA to yield BPEA-PMMA, DBT-PMMA, and NiR-PMMA films, which exhibit cyan, yellow, and red fluorescence, respectively. Fluo, with water solubility, was incorporated into PVB to prepare Fluo-PVB film, emitting bright green fluorescence. Notably, all these fluorescent films have high photoluminescence quantum yields: 90.7% (cyan), 50.8% (green), 86.5% (yellow), and 52.5% (red) (Figs. S3 and S4).

Good spectral overlap and high quantum yield are prerequisites for efficient energy transfer. There are generally two types of energy transfer: radiative energy transfer and nonradiative energy transfer. FRET, as a non-radiative energy transfer process mediated by long-range dipole-dipole interactions, requires not only matching energy levels but also close distances (< ~10 nm) and appropriate orientation between donors and acceptors[26]. FRET often sacrifices lifetime. In contrast, radiative energy transfer only requires satisfying spectral overlap, making it a more convenient method. Moreover, the luminescence lifetime of the donor remains unchanged. Realization of this concept would simplify the creation of multi-color ultralong afterglow, bypassing compatibility concerns between disparate luminophores and their respective

matrices. To verify this hypothesis, two types of composite films were fabricated, each predicated on distinct energy transfer mechanisms: a double-layered film (named "TP-dye" film) based on radiative energy transfer and a blend film (named "TP@dye" film) based on FRET. In the double-layered film system, exemplified by the TP-BPEA double-layered film, the delayed spectrum exhibited not only the characteristic blue emission of TP-PVA at 473 nm but also a new cyan peaking at approximately 500 nm (Fig. 2d). The Commission International de l'Eclairage (CIE) coordinates showed that the delayed emission changed from deep blue to cyan (Fig. 2e). The cyan delayed emission aligned well with the fluorescence peak of BPEA-PMMA, attributed to the radiation transition from S_1 state of BPEA (Fig. S4). Moreover, the lifetime at 500 nm was 6.99 s (Fig. 2f), which is consistent with the lifetime of TP-PVA. These observations confirm the existence of radiative energy transfer process between TP and BPEA. Analogous results were obtained in TP-Fluo, TP-DBT, and TP-NiR double-layered films, yielding ultralong lifetime emissions in cyan (τ = 6.39 s), yellow (τ = 6.76 s), and red (τ = 6.05 s) colors. Furthermore, since the absorption spectrum of NiR and the emission spectrum of DBT overlap well, a tripled-layered film comprising TP-PVA, DBT-PMMA, and NiR-PMMA was constructed. Through cascaded radiative energy transfer, white light emission with CIE coordinates (0.32, 0.32) was achieved (Fig. S8). In the blend film system, such as TP@Fluo film, the lifetime decreased to 2.04 s, even though a delayed peak attributed to Fluo's green emission can be observed in the delayed spectrum, and the afterglow changed from blue to green (Fig. S9). This trend was also observed in the TP@DBT and TP@NiR blend films, where the lifetimes of the yellow and red delayed peaks reduced to 1.84 and 1.27 s (Figs. S10 and S11). These findings suggested that the FRET mechanism present in the blend films realized tunable emission while losing the advantage of ultralong lifetime emission. Unfortunately, the spectral performance of BPEA in the blend film (TP@BPEA) could not be compared to that in the double-layered film (TP-BPEA) due to significant polarity differences between PMMA and PVA matrices, which affect the emission characteristics. This incompatibility highlights an advantage of the double-layered approach, as it circumvents concerns regarding chromophore-matrix and chromophore-chromophore compatibility. Collectively, these observations demonstrate that the

double-layered method based on radiative energy transfer can be used to create multi-color ultralong afterglow systems in an easy, universal, and efficient way.

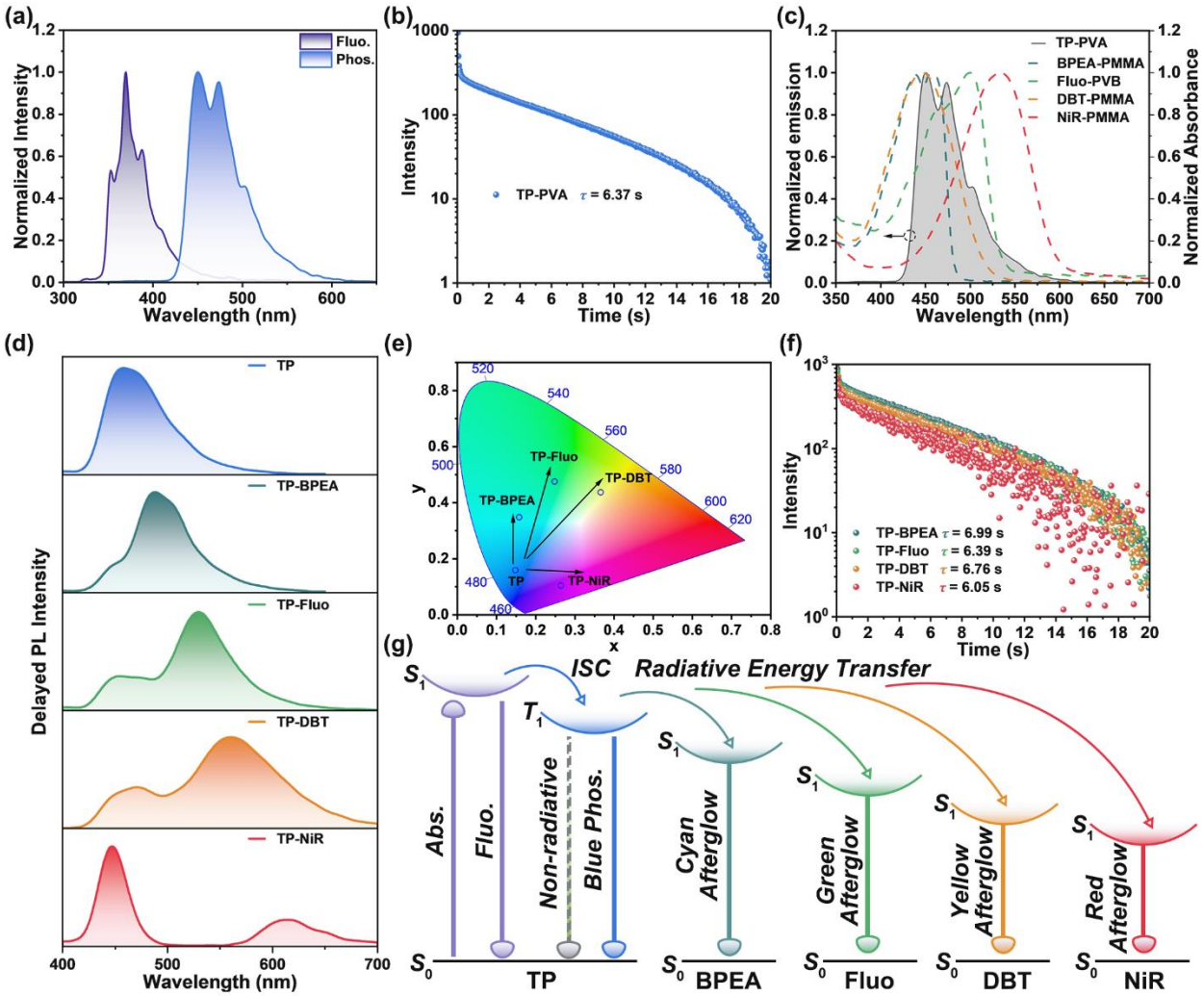

Fig. 2: Photophysical properties of the OU-RTP films and multi-color luminescent films under ambient condition. (a) Prompt spectrum and delayed spectrum of TP-PVA film under (TP:PVA = 3:1000, w/w, λ_{ex} = 254 nm). (b) Decay curve of TP-PVA film (λ_{ex} = 254 nm, λ_{em} = 475 nm). (c) Delayed spectrum of TP-PVA film and absorption spectra of BPEA-PMMA, Fluo-PVB, DBT-PMMA, and NiR-PMMA films. (d) Delayed spectrum of TP-PVA film, TP-Fluo film, TP-DBT film, and TP-NiR film under ambient

conditions (λ_{ex} = 254 nm). (e) Simplified Jablonski diagram to explain the possible mechanism for the radiative energy transfer process. Abs. = absorption, Fluo. = fluorescence, Phos. = phosphorescence.

Construction Organic CPA Materials with CLCs. CLCs, characterized by their periodic helical superstructures, can selectively reflect circularly polarized light at wavelengths that satisfy the Bragg equation and align with the helix orientation, while allowing other incident light to pass through. Therefore, they can be used to construct CPL materials. This selective reflection characteristic forms the photonic bandgap (PBG) of the CLCs. The PBG of the materials can be manipulated by adjusting the concentration of chiral dopants, thus controlling the color of the reflected light. The liquid crystal mixture E7, known for its wide working temperature range and high birefringence, was selected as the liquid crystal matrix. Thereby, periodic helical superstructures with different orientations and pitches were achieved by incorporating varying quantities of chiral dopants (*R*/*S*-5011). As shown in Figs. S12–S15, a PBG distribution across the entire visible spectrum from 450 nm to 700 nm was obtained, manifesting as blue, cyan, green, yellow, and red reflective colors in polarizing optical microscopy (POM) images. For nomenclature, samples are prefixed with "ES" or "ER" to denote the chirality of dopants (*S*-5011 or *R*-5011), followed by the reflected color, e.g., ES-Blue for blue-reflecting CLCs derived from E7 doped with *S*-5011. Circular dichroism (CD) spectroscopy was employed to characterize the CLCs. As seen in Fig. S16, ES-Blue demonstrated an intense positive CD signal beyond the detection limit across 395-544 nm, with a distinct negative signal at 330 nm matching the absorption profile of E7 (Figs. S17 and S18). A strong negative CD signal was observed for ER-Blue within the blue band too. The integration of the ultralong lifetime TP-PVA film with ER-Blue resulted in a superior CPL signal with a high g_{lum} value of +1.90, reaching a high level in the pure organic CPA domain. Likewise, the combination of the cyan-luminescent TP-BPEA bilayer with ES-Cyan resulted in a CPL negative signal with a g_{lum} value of -1.79. Employing this method, multicolored optically active CPA materials were synthesized, featuring exceptional g_{lum} values across the visible spectrum, as detailed in Table 1 and Fig. S20. Our approach, leveraging the

selective reflection of CLCs and multi-layered assembly strategy based on radiative energy transfer, has successfully yielded multicolored pure organic CPA materials with ultrahigh g_{lum} values.

Table 1. The g_{lum} values of the composite materials of multi-color ultralong afterglow films and their corresponding CLC layers.

Sample	ER/S-TP	ER/S-TP-BPEA	ER/S-TP-Fluo	ER/S-TP-DBT	ER/S-TP-NiR
g_{lum}	+1.90/-1.81	+1.56/-1.79	+1.52/-1.85	+1.52/-1.47	+1.56/-1.16

Construction Organic CPA Materials with CLCPs. The feasibility of this strategy is confirmed, yet the inherent fluidity of CLCs hinders their widespread application. CLCP films, known for their high flexibility and bendability, can compensate for this shortcoming. The preparation method for CLCP films is as follows: the reactive liquid crystal (LC) monomers, chiral dopants, and photoinitiators were homogeneously dissolved in dichloromethane. After the solvent slowly evaporated, the resultant mixture was injected into a liquid crystal cell at 75°C. After exposure to a 365 nm UV lamp at 1.5 mW·cm^{-2} for 10 minutes, the CLC polymerized to form a CLCP film. The resulting films were peeled off for further analysis (Fig. 3a). By varying the chiral dopant concentration, a series of "LR/S-color" CLCP films were obtained, each reflecting a distinct color across the visible spectrum (Fig. 3b) and named accordingly. LS-Blue, for example, indicates a CLCP film doped with a certain proportion of *S*-5011 to reflect blue light.

As shown in Fig. 3d, LS-Blue exhibited uniform morphology and blue color under POM. Further cross-sectional scanning electron microscopy (SEM) analyses revealed uniform and regular layered structures formed (Fig. 3c). The optical properties were studied by CD spectroscopy (Fig. 3d), with the LR-Blue film demonstrating an intense negative CD signal ranging from 370 to 515 nm, while LS-Blue showed a strong positive CD signal over the same wavelength range, indicating successful chiral induction in the CLCP films.

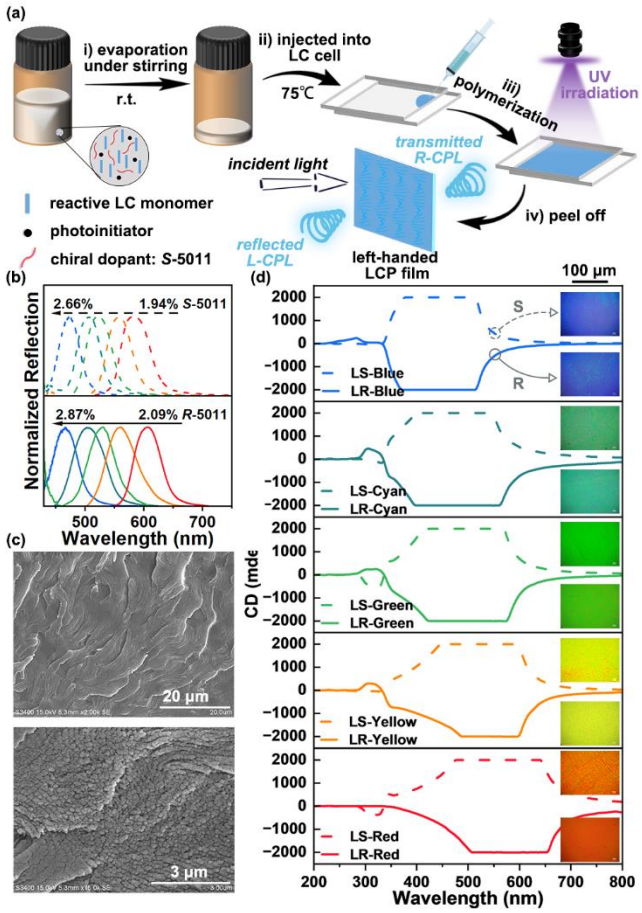

Fig. 3. Structural and photophysical properties of CLCP films. (a) Schematic illustration of the preparation process of CLCP films. (b) Normalized reflection spectra of CLCP films doped with different ratios of *S*/*R*-5011. (c) Cross-sectional SEM images of CLCP film (the scale bar in the SEM image above is 20 μm, and the below is 3 μm). (d) CD spectra of CLCP films doped with different ratios of *S*/*R*-5011. Inset: POM images of the CLCP film doped with different ratios of *S*/*R*-5011.

Subsequently, TP-PVA was integrated with LR-Blue and LS-Blue to fabricate multi-layered films, which were named as TP-LR-Blue and TP-LS-Blue, respectively. These films produced intense blue CPL signals with g_{lum} values of +1.50 and -1.24 at 475 nm, respectively. These values were slightly lower than the CLC system discussed previously, which may be attributed to the smoother surface and enhanced selective reflection capability of CLCs. Nevertheless, the g_{lum} values here surpass most reported optically active pure

organic CPA systems by two orders of magnitude. Employing this assembly method, our findings were successfully extended to cyan, green, yellow, and red CPA, each with high $|g_{lum}|$ values: +1.67/-1.40, +0.95/-1.55, +1.17/-1.51, and +1.23/-0.95, respectively (Figs. 4a and 4b). As shown in Fig. 4c, the multi-layered film exhibited a significant CPL signal. To validate the uniformity of films, CPL spectra and g_{lum} values at three different regions of TP-Fluo-LS-Green film were measured, finding nearly identical results across all areas (Fig. 4d). The strategy of integrating ultralong luminescent films with CLCP films has been proven effective for creating uniformly high-quality CPA films across the visible spectrum. To investigate whether the addition of CLCP films affects the overall lifetime of the multi-layered films, we measured the delayed emission lifetimes of the triple-layered films and found that they still maintained a lifetime of more than 6 s (Figs. 4e and S29-33).

To further explore the underlying mechanism, the CPL spectra of multi-layered films with varying layer sequences were investigated, focusing on the TP-NiR system with the largest Stokes shift. Three distinct configurations based on their proximity to the excitation source were examined (Fig. 4f): (I) TP-PVA, NiR-PMMA, LR-Red; (II) TP-PVA, LR-Blue, NiR-PMMA; (III) LR-Red, TP-PVA, NiR-PMMA. In configuration I, TP-PVA film was excited by UV light, emitting blue phosphorescence that induced persistent red fluorescence from NiR-PMMA. This red emission aligned with the PBG of LR-Red, leading to the selective reflection of red *R*-type CPL and the transmission of *S*-type CPL. Consequently, this resulted in a strong positive red CPL signal with a g_{lum} value of 1.21. In configuration II, the UV-induced blue phosphorescence was initially converted to blue *S*-type CPL by the LR-Blue film. However, the detector only received a positive blue CPL signal with a high g_{lum} value of 1.40, without any red CPL signal. This observation suggests that, in this configuration, although the blue CPL can induce red fluorescence from NiR-PMMA, it fails to stimulate red CPL signals, indicating that the "CPL excitation" strategy is ineffective in this scenario. In configuration III, UV light passed through LR-Red first, then through TP-PVA and NiR-PMMA. Notably, the CPL signal reversed, resulting in a negative red CPL signal with a g_{lum} value of 0.18. We speculated that the red emission from TP-NiR, upon incidence on the LR-Red surface, prompted LR-

Red to reflect R-type red CPL towards the detector, thereby generating a weaker negative red CPL signal. These findings offered an efficient and versatile method for CPL regulation.

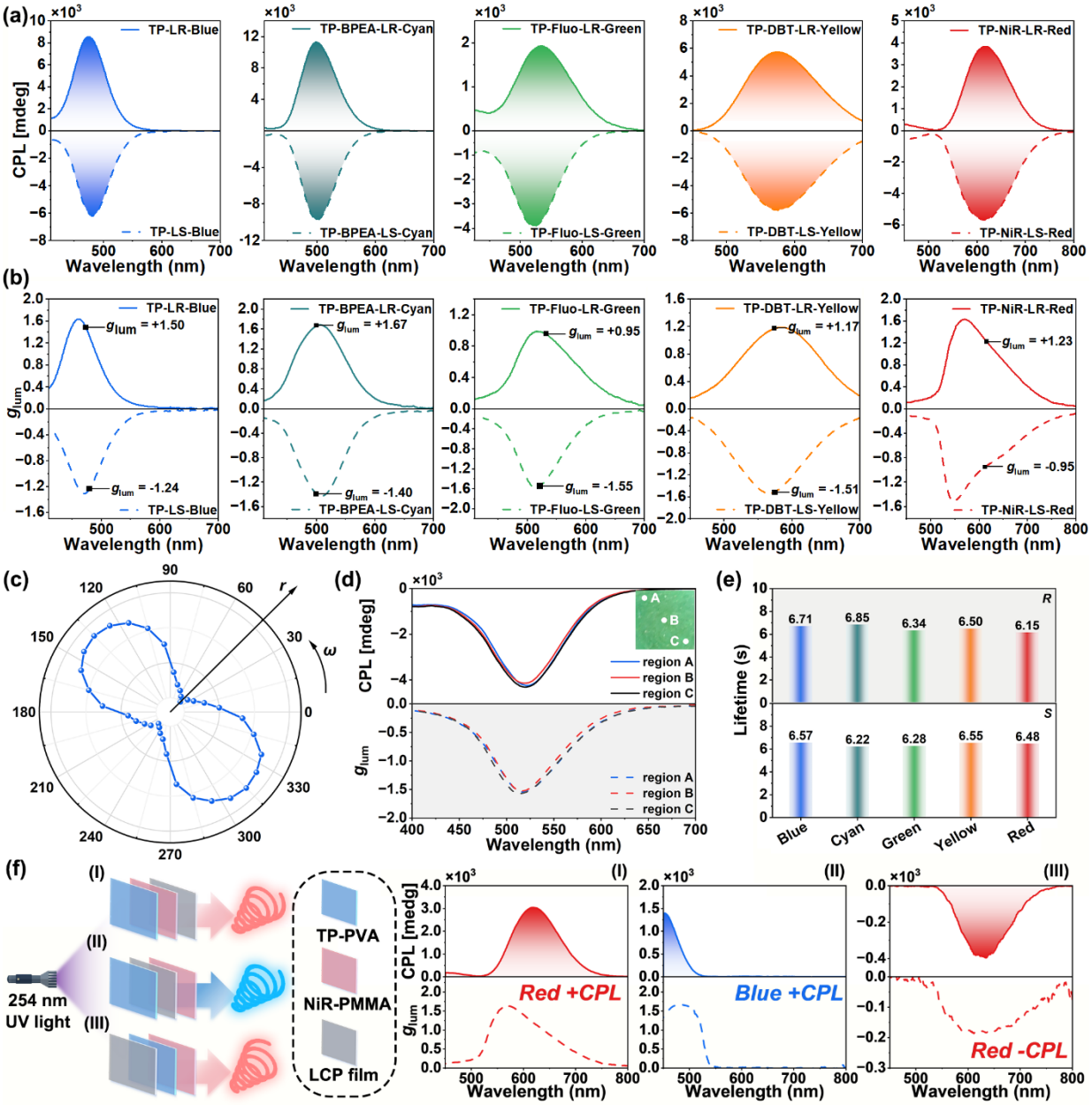

Fig. 4. Photophysical properties of the triple-layered composite films under ambient conditions. (a) CPL spectra and (b) g_{lum} spectra of the triple-layered composite films (λ_{ex} = 254 nm). (c) The angle-dependent emission intensity (r) at 475 nm of TP-LS-Blue film. The polar angle ω is the orientation angle

of the liner polarizer relative to the quarter-wave plate (see Fig. S23). (d) CPL spectra of TP-Fluo-LS-Green film at different regions. (e) The lifetimes of the triple-layered composite films (λ_{ex} = 254 nm, delay time = 0.1 ms). (f) Illustration of three different CPL generation channels based on different layer sequences: (I) TP-PVA, NiR-PMMA, LR-Red; (II) TP-PVA, LR-Blue, NiR-PMMA; (III) LR-Red, TP-PVA, NiR-PMMA.

Applications of pure organic CPA materials. The time-dependent afterglow and polarization signals of the pure organic CPA films were harnessed to explore its application in multi-level information encryption. As illustrated in Fig. 5, a hidden message with multi-level encryption was encoded using five distinct films: NiR, TP@NiR, TP-NiR, TP-NiR-LR-Red, and TP-NiR-LS-Red. Under 254 nm UV light, the initial code "8888" was exposed. With the UV light extinguished, a second code "8028" emerged. Further inspection with left- or right- handed circular polarized filter (*L*/*R*-CPF) yielded preliminary passwords "8726" and "802H", which were not the true codes yet. After the UV light was turned off for 10 s, an additional hidden code "2029" was unveiled. Subsequently, by observing through the *R*-CPF, the correct code "2024" was displayed. Conversely, employing the *L*-CPF would yield the error code "2725". Thus, the only correct information "2024" was exclusively accessible after 10-second interval following UV light cessation and *R*-CPF observation. Deviations in timing or polarization would lead to the retrieval of incorrect passwords. These results suggest that the pure organic CPA materials, fabricated with multi-layered films, holds significant potential for applications in anti-counterfeiting and encryption.

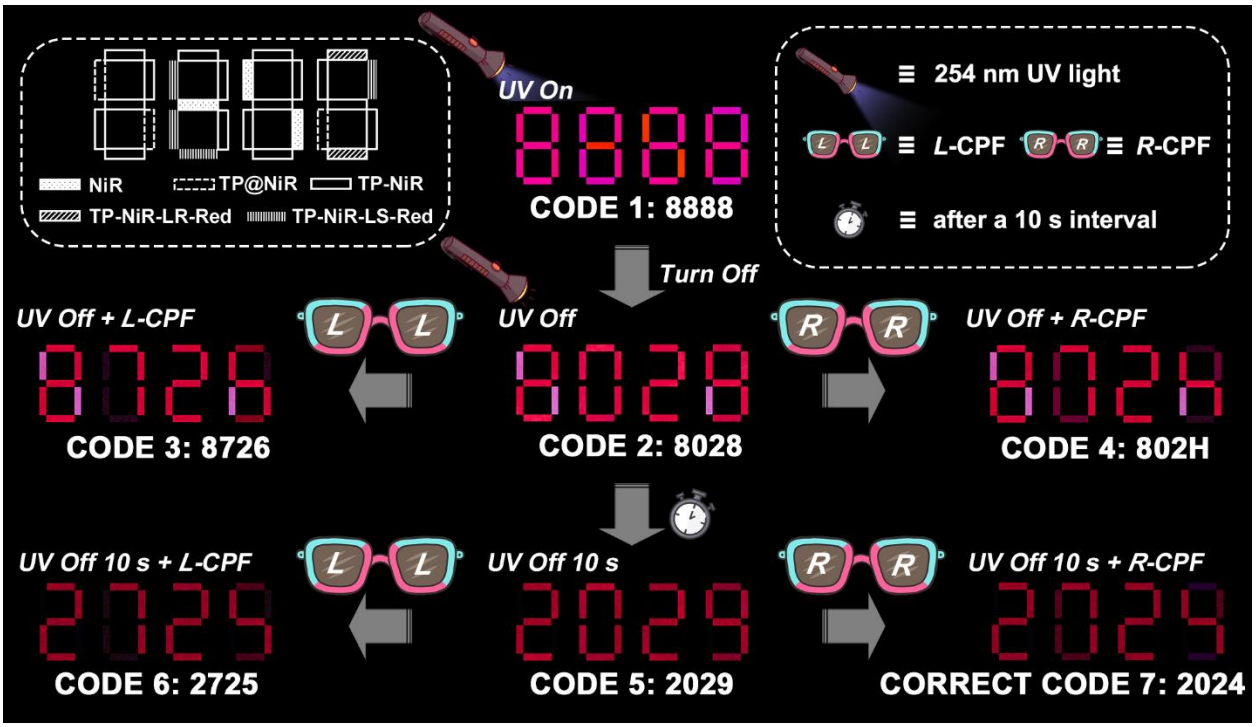

Fig. 5. Application of pure organic CPA materials. Construction and decryption of a multi-level information encryption system based on NiR, TP@NiR, TP-NiR, TP-NiR-LR-Red, and TP-NiR-LS-Red films. One layout can yield seven different codes when viewed at different timings and through different polarizers.

Discussion

In summary, this study introduces a novel approach employing radiative energy transfer and the selective reflection of CLCPs to develop full-color pure organic CPA materials across the entire visible spectrum. By rearranging the assembly sequence of multi-layered films, the wavelength and polarization direction of the CPL could be effectively modulated. Furthermore, time-dependent luminescence and polarization characteristics of the CPA materials enable the establishment of multi-dimensional optical encryption. This straightforward self-assembly strategy of multi-layered films holds promise for advanced applications in information security and anti-counterfeiting technologies.

Methods

Materials. Triphenylen-2-ylboronic acid (TP), fluorescein sodium (Fluo), *R*-5011, *S*-5011, and poly(vinyl alcohol) (PVA) were purchased from Adamas beta. 9,10-bis(phenylethynyl)anthracene (BPEA) and 4,7-di(thiophen-2-yl)benzo[*c*][1,2,5]thiadiazole (DBT) was purchased from Leyan. Poly(methyl methacrylate) (PMMA) was purchased from Meryer. Nile red (NiR) was purchased from Meryer. The commercial LCP was purchased from Nanjing Ningcui Optical Technology Co., Ltd. These reagents were used as supplied without further purification unless otherwise indicated. All other reagents were commercially available and used as supplied without further purification. Ultrapure water was obtained using a Direct-Pure UP UV 10 machine.

General methods. Ultraviolet–visible (UV–vis) absorption spectra were obtained on an Agilent Cary 60 spectrophotometer (Agilent Technologies). Prompt spectra, delayed spectra (delay time = 0.1 ms, gate time = 20 ms) and luminescence decay curves were acquired using an Agilent Cary Eclipse fluorescence spectrophotometer (Agilent Technologies). Quantum yields were measured using an integrating sphere on a HAMAMATSU Quantaurus-QY C11347-11. Circularly polarized luminescence (CPL) spectra were acquired using a JASCO CPL-200 spectrophotometer. Circular dichroism (CD) spectra were acquired using JASCO J815 and J1500 spectrophotometers. The optical textures of LC samples were observed by a polarized optical microscope (POM) (LVPOL 100, Nikon) with crossed polarizers under reflection mode and were recorded using a charge-coupled device (CCD) camera. Generally, the fiber-coupled spectrometer (Avaspec-ULS2048, resolution: 2 nm, 200-1100 nm) was used to detect the reflection spectra. The CIE coordinates were calculated using Chromaticity Diagram application running in OriginPro 2024b environment. Scanning electron microcopy (SEM) images were obtained by using a S-3400N (Hitachi) (the sample was coated with nano Au in a vacuum). Digital photos were recorded by a Canon EOS 700D camera and a Canon EF 35 mm f/2 IS USM lens with a NiSi H MC UV 67 mm filter.

Data Availability

All relevant data that support the findings are available within this article and supporting information and are also available from authors upon reasonable request.

References

1. He, T., Guo, W.-J., Chen, Y.-Z., Yang, X.-F., Tung, C.-H. & Wu, L.-Z. Ratiometric hypoxia detection by bright organic room temperature phosphorescence of uniformed silica nanoparticles in water. *Aggregate* **4**, e250 (2022).
2. Zhou, X., Bai, X., Shang, F., Zhang, H.-Y., Wang, L.-H., Xu, X. & Liu, Y. Supramolecular assembly activated single-molecule phosphorescence resonance energy transfer for near-infrared targeted cell imaging. *Nature Communications* **15**, 4787 (2024).
3. Guo, W.-J., Chen, Y.-Z., Tung, C.-H. & Wu, L.-Z. Ultralong Room-Temperature Phosphorescence of Silicon-Based Pure Organic Crystal for Oxygen Sensing. *CCS Chemistry* **4**, 1007-1015 (2022).
4. Si, C., Wang, T., Gupta, A. K., Cordes, D. B., Slawin, A. M. Z., Siegel, J. S. & Zysman – Colman, E. Room-Temperature Multiple Phosphorescence from Functionalized Corannulenes: Temperature Sensing and Afterglow Organic Light-Emitting Diode. *Angewandte Chemie International Edition* **62**, e202309718 (2023).
5. Zou, X., Gan, N., Dong, M., Huo, W., Lv, A., Yao, X., Yin, C., Zhang, Z., Zhang, Y., Chen, H., Ma, H., Gu, L., An, Z. & Huang, W. Narrowband Organic Afterglow via Phosphorescence Förster Resonance Energy Transfer for Multifunctional Applications. *Advanced Materials* **35**, 2210489 (2023).
6. Jiang, S., Guo, D., Lin, F., Chen, J., Miao, Y., Huang, H., Yang, J.-W., Qin, W. & Chi, Z. Time-Dependent Multicolor Afterglow from Dual Persistent Luminescence of Fluorescence and Phosphorescence in a UV-Cured Polyurethane Matrix. *ACS Materials Letters* **6**, 1371-1379 (2024).
7. Yang, F., Yue, B. & Zhu, L. Light-triggered Modulation of Supramolecular Chirality. *Chemistry – A European Journal* **29**, e202203794 (2023).

8. Hao, W., Wang, Y. & Liu, M. Nonaromatic Lysine Supramolecular Nanotube Assemblies with Excitation-Dependent Circularly Polarized Phosphorescence. *ACS Materials Letters* **6**, 3487-3495 (2024).

9. Yang, B., Yan, S., Zhang, Y., Ban, S., Ma, H., Feng, F. & Huang, W. Double-Model Decay Strategy Integrating Persistent Photogenic Radicaloids with Dynamic Circularly Polarized Doublet Radiance and Triplet Afterglow. *Journal of the American Chemical Society* **146**, 7668-7678 (2024).

10. He, Z., Huang, Z. & Ma, X. Lifetime-tunable circularly polarized luminescent system based on triplet-to-singlet Förster resonance energy transfer. *Science China Chemistry*, DOI: 10.1007/s11426-024-1993-4 (2024).

11. Gu, L., Ye, W., Liang, X., Lv., A., Ma, H., Singh, M., Jia, W., Shen, Z., Guo, Y., Gao, Y., Chen, H., Wang, D., Wu, Y., Liu, J., Wang, H., Zheng, Y.-X., An, Z., Huang, W. & Zhao, Y. Circularly Polarized Organic Room Temperature Phosphorescence from Amorphous Copolymers. *Journal of the American Chemical Society* **143**, 18527-18535 (2021).

12. Wei, L., Guo, S., Zhang, B., Jiang, B., Wang, Y., Liu, Z., Xu, Y., Gong, Y., Liu, Y. & Yuan, W. Z. Tuning Circularly Polarized Afterglow Color via Modulation of Energy and Chirality Transfer in Co-Doped Films. *Advanced Functional Materials*, DOI: 10.1002/adfm.202409681 (2024).

13. Nie, F., Wang, K.-Z. & Yan, D. Supramolecular glasses with color-tunable circularly polarized afterglow through evaporation-induced self-assembly of chiral metal-organic complexes. *Nature Communications* **14**, 1654 (2023).

14. Guang, L., Lu, Y., Zhang, Y., Liao, R. & Wang, F. Circularly Polarized Phosphorescence of Benzils Achieved by Chiral Supramolecular Polymerization. *Angewandte Chemie International Edition* **63**, e202315362 (2024).

15. Wang, Y., Li, N., Chu, L., Hao, Z., Chen, J., Huang, J., Yan, J., Bian, H., Duan, P., Liu, J. & Fang, Y. Dual Enhancement of Phosphorescence and Circularly Polarized Luminescence through Entropically Driven Self-Assembly of a Platinum(II) Complex. *Angewandte Chemie International Edition* **63**, e202403898 (2024).

16. Zhong, H., Gao, X., Zhao, B. & Deng J. "Matching Rule" for Generation, Modulation and Amplification of Circularly Polarized Luminescence. *Accounts of Chemical Research* **57**, 1188-1201 (2024).

17. Wu, Y., Li, M., Zheng, Z.-g., Yu, Z.-Q. & Zhu, W.-H. Liquid Crystal Assembly for Ultra-dissymmetric Circularly Polarized Luminescence and Beyond. *Journal of the American Chemical Society* **145**, 12951-12966 (2023).

18. Yu, F., Liu, S., Liu, X., Zhang, H., Zheng, Z., Zhu, W.-H. & Wu, Y. Circularly Polarized Perovskite Luminescence in Composite Films with High Flexibility and Stability. *Advanced Optical Materials* **145**, 2400411 (2024).

19. Liu, J., Wu., J.-J., Wei, J., Huang, Z.-J., Zhou, X.-Y., Bao, J.-Y., Lan, R.-C., Ma, Y., Li, B.-X., Yang, H., Lu, Y.-Q. & Zhao, Q. Dynamically Modulating the Dissymmetry Factor of Circularly Polarized Organic Ultralong Room-Temperature Phosphorescence from Soft Helical Superstructures. *Angewandte Chemie International Edition* **63**, e202319536 (2024).

20. Wang, X., Zhao, B. & Deng J. Liquid Crystals Doped with Chiral Fluorescent Polymer: Multi-Color Circularly Polarized Fluorescence and Room-Temperature Phosphorescence with High Dissymmetry Factor and Anti-Counterfeiting Application. *Advanced Materials* **35**, 2304405 (2023).

21. Liu, J., Song, Z.-P., Wei, J., Wu, J.-J., Wang, M.-Z., Li, J.-G., Ma, Y., Li, B.-X., Lu, Y.-Q. & Zhao, Q. Circularly Polarized Organic Ultralong Room-Temperature Phosphorescence with A High Dissymmetry Factor in Chiral Helical Superstructures. *Advanced Materials* **36**, 2306834 (2023).

22. Wang, X., Yang, K., Zhao, B. & Deng, J. Polymeric Cholesteric Superhelix Induced by Chiral Helical Polymer for Achieving Full-Color Circularly Polarized Room-Temperature Phosphorescence with Ultra-High Dissymmetry Factor. *Small*, DOI: 10.1002/smll.202404576 (2024).

23. Ma, L., Xu, Q., Sun, S., Ding, B., Huang, Z.， Ma, X. & Tian, H. A Universal Strategy for Tunable Persistent Luminescent Materials via Radiative Energy Transfer. *Angewandte Chemie International Edition* **61**, e202115748 (2022).

24. Cheng. A., Su, H., Gu, X., Zhang, W., Zhang, B., Zhou, M., Jiang, J., Zhang, X. & Zhang, G. Disorder-Enhanced Charge-Transfer-Mediated Room-Temperature Phosphorescence in Polymer Media. *Angewandte Chemie International Edition* **62**, e202312627 (2023).

25. Li, D., Yang, J., Fang, M., Tang, B. Z. & Li, Z. Stimulus-responsive room temperature phosphorescence materials with full-color tunability from pure organic amorphous polymers. *Science Advances* **8**, eabl8392 (2022).

26. Zeng, M., Wang, W., Zhang, S., Gao, Z., Yan, Y., Liu, Y., Qi, Y., Yan, X., Zhao, W., Zhang, X., Guo, N., Li, H., Li, H., Xie, G., Tao, Y., Chen, R. & Huang, W. Enabling robust blue circularly polarized organic afterglow through self-confining isolated chiral chromophore. *Nature Communications* **15**, 3053 (2024).

27. Xu, D., Liu, C., Li, H., Cheng, Y. & Zheng, W.-H. Circularly Polarized Room Temperature Phosphorescence of Chiral Bromoxanthone Using a Chiral Self-Assembled Liquid Crystal Polymer Frameworks. *Advanced Optical Materials* **12**, 2303019 (2024).

28. Gong, W., Huang, G., Yuan, Y. & Zhang, H. Strong and Multicolor-Tunable Pure Organic Circularly Polarized Room-Temperature Phosphorescence from Cholesteric Liquid Crystal. *Advanced Optical Materials* **11**, 2300745 (2023).

29. Gong, W., Zhou, M., Xiao, L., Fan, C., Yuan, Y., Gong, Y. & Zhang, H. Multicolor-Tunable and Time-Dependent Circularly Polarized Room-Temperature Phosphorescence from Liquid Crystal Copolymers. *Advanced Optical Materials* **12**, 2301922 (2023).

30. Jiang, K., Fan, Q., Guo, D., Song, C. & Guo, J. Circularly Polarized Room-Temperature Phosphorescence with an Ultrahigh Dissymmetry Factor from Carbonized Polymer Dots by Stacked Chiral Photonic Films. *ACS Applied Materials & Interfaces* **15**, 26037-26046 (2023).

31. Huang, A., Huang, J., Luo, H.-Y., Luo, Z.-W., Wang, P., Wang, P., Guan, Y. & Xie, H.-L. Circularly polarized organic room temperature phosphorescence activated by liquid crystalline polymer networks. *Journal of Materials Chemistry C* **11**, 4104-4111 (2023).

32. Zhang, D.-W., Li, M. & Chen, C.-F. Axially chiral materials exhibiting blue-emissive ultralong organic phosphorescence and intense circularly polarized luminescence. *Science China Materials* **66**, 4030-4036 (2023).

33. Fan, Q., Li, Z., Jiang, K., Gao, J., Lin, S. & Guo, J. Tunable circular polarization room temperature phosphorescence with ultrahigh dissymmetric factor by cholesteric liquid crystal elastomers. *Cell Reports Physical Science* **4**, 101583 (2023).

34. Wang. X., Miao, Q., Zhang, W., Zhou, Y., Xiong, R., Duan, Y., Meng, X. & Ye, C. Switchable circular polarized phosphorescence enabled by cholesteric assembled nanocelluloses. *Chemical Engineering Journal* **481**, 148463 (2024).

35. Xu, M., Wu, X., Yang, Y., Ma, C., Li, W., Yu, H., Chen, Z., Li, J., Zhang, K. & Liu, S. Designing Hybrid Chiral Photonic Films with Circularly Polarized Room-Temperature Phosphorescence. *ACS Nano* **14**, 11130-11139 (2020).

36. Zhang, D., Zheng, H., Ma, X., Su, L., Gao, X., Tang, Z. & Xu, Y. On-Demand Circularly Polarized Room-Temperature Phosphorescence in Chiral Nematic Nanoporous Silica Films. *Advanced Optical Materials* **10**, 2102015 (2022).

37. Cao, M., Ren, Y., Wu, Y., Shen, J., Li, S., Yu, Z.-Q., Liu, S., Li, J., Rojas, O. J. & Chen, Z. Biobased and biodegradable films exhibiting circularly polarized room temperature phosphorescence. *Nature Communications* **15**, 2375 (2024).

Acknowledgements

We gratefully acknowledge the financial support from the National Key Research and Development Program of China (2022YFB3203500), National Natural Science Foundation of China (22125803, and 22020102006), and Fundamental Research Funds for the Central Universities.

Author contributions

Conceptualization: C. Yin, Z.-A. Yan, X. Ma

Methodology: C. Yin, Z.-A. Yan, H. Hu

Investigation: C. Yin, Z. Xu

Visualization: C. Yin, P. Jiang

Supervision: X. Ma, H. Tian

Writing—original draft: C. Yin

Writing—review & editing: C. Yin, Z.-A. Yan, X. Ma, H. Tian

Competing interests

The authors declare no competing interests.